RSC Advances

ROYAL SOCIETY OF CHEMISTRY

www.rsc.org/advances

RSC Advances

RSC Publishing

COMMUNICATION

Cite this: DOI: 10.1039/x0xx00000x

Received 00th January 2012,
Accepted 00th January 2012

DOI: 10.1039/x0xx00000x

www.rsc.org/

Facile hydrothermally selective fabrication of $Ni(OH)_2$ and $Ni(HCO_3)_2$ nanoparticulates and their electrochemical performances

Yinan Yan,[a] Gang Cheng,[b*] Ping Wang[a], Dannong He [a*], and Rong Chen [b*]

Cone-like, flower-like nickel hydroxide, and sphere-like nickel bicarbonate were synthesized via a simple hydrothermal route by varying the amounts of urea, without addition of any surfactants or additives. The surface areas of obtained materials are measured to be 17.3 m^2 g^{-1}, 45.7 m^2 g^{-1} and 39.9 m^2 g^{-1}, and correlated electrochemical performances were briefly investigated. The maximum specific capacitance was recorded to be 1429.3 F g^{-1} in sphere-like nickel bicarbonate nanoparticles, suggesting its potential application in supercapacitor electrode.

Introduction

The depletion of fossil fuel and severe environmental pollution stimulate the research developing into new sustainable energy sources and rechargeable devices [1]. On account of advantages as elevated efficiency, superior power and lengthy cycle life, supercapacitor is considered to be one of the most promising devices for bridging gap between traditional physical capacitors and battery cells to satisfy market requirement [2]. The main active ingredient on supercapacitor electrodes is divided into two categories: the electrical double-layer capacitors (EDLC) materials and the pseudo-capacitors materials. Associated with the EDLC-type carbon materials (usually less than 300 F g^{-1}) [3], transition metal oxides and hydroxides result in substantially larger specific capacitance from valence-reversible faradaic reactions [4,5].

Nickel compounds have been regarded as promising electrode materials among the numerous pseudo-capacitance storage materials. In the past decade, varieties of synthetic methods such as chemical precipitation, hydrothermal reaction, electrochemical deposition, and sol-gel processes from different precursors, had been exploited to prepare nickel compound nanoparticles [6-10]. Among the above approaches, hydrothermal method, with the ability to dissolve and recrystallize normally insoluble materials under high pressure and temperature conditions, possesses the advantages of easy-handling, energy-saving, simplicity and cost effectiveness. However, the agents utilized for precipitation in hydrothermal reaction greatly affect the size, the crystallinity, the surface and the related electrochemical performance [11]. Immediate precipitation by neutralizing nickel ions with hydroxide ions, also called "direct precipitation route (DP)", is a conventional synthetic technique at early stage. The capacity of DP method-made nickel hydroxide is usually less than 576 F g^{-1} due to the limited surface of size-varied large particles [12]. Modified "coordination homogeneous precipitation (CHP)" method was developed with the purpose of reaching granular uniformity. Affected by coordination agents such as ammonium water, sodium succinate, ethylene-diamine-tetra acetic acid, sodium potassium tartrate and tri-ethanol amine, nickel ions would precipitate homogeneously in extended sedimentation time [13]. Moreover, complex and versatile structures could be fabricated by the involvement of surfactants through CHP method via hydrothermal route. In presence of sodium dodecyl sulphate, PEG-400 or Tween-80, the platelet-like particles from ammonium water coordination varied into cone-like, thin-flake-like or need-like ones, [14-16]. Tube-like nickel oxide with diameter in range of 60-80 nm was also successively fabricated under the intervention of anion surfactants. The enlarged surface area, reduced particle size and shorten diffusion path effectively improved their electrochemical performances [17].

Prolonging release of hydroxyl-ion during ureolysis at elevated temperature is helpful for yielding smaller particles in nano-size, and is generally classified as "urea homogeneous precipitation (UHP)" method. Herein, we report a facile hydrothermal approach to prepare versatile nickel nanoparticulates by simply altering the concentration of urea without involving of surfactants, in which carbonate and ammonium ions from the decomposition of urea could react with nickel ions to form $Ni(OH)_2$, $Ni(HCO_3)_2$ or mixtures. The crystal phase, structure, surface area, and correlated electrochemical properties of synthesized nanoparticulates were also investigated in this paper.

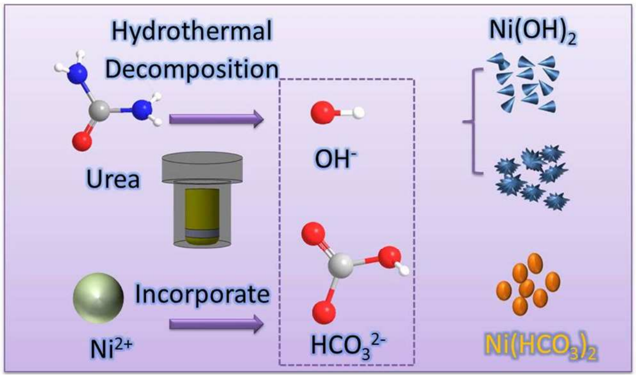

Scheme.1 Illustration for the formation of nickel-based nanoparclutates.

Experimental Section

The atomic mole ratios of nickel nitrate to urea were set to be 1:1, 1:2, 1:3, 1:5 and 1:10. In a typical procedure, 2 mmol nickel nitrate hexhydrate ($Ni(NO_3)_2$ $6H_2O$) and urea were added into de-ionized water, followed by magnetically stirring for 2 hours at 60°C in water bath to form homogeneous solutions. The mixture solutions were transferred into 50 mL Teflon-lined autoclaves and kept at 180°C for 12 h. The autoclaves were allowed to cool in ambient temperature, and the precipitates were collected and washed with de-ionized water and ethanol several times by centrifugation, then dried at 60°C. The names of as-prepared samples were designated as S1, S2, S3, S4 and S5 respectively according to urea amount (2, 4, 6, 10 and 20 mmol).

Samples from UHP method were characterized via various techniques. X-ray diffraction (XRD) measurements were performed using a D8 Advance (Bruker, Germany) at room temperature in specular reflection mode with Cu/Kα radiation. SEM images were taken on a field-emission electron microscope S4800 operating at an acceleration voltage of 3 or 5kV. TEM images and SAED patterns were recorded on a JEOL 2010 electron microscope, using an accelerating voltage of 200 kV. The isotherm of nitrogen physical-adsorption was obtained using an ASAP-2020 surface analyser (Micromeritics instruments, USA), and the specific surface area (SSA) was determined by the Brunauer-Emmett-Teller (BET) method.

Electrochemical performance was recorded by computer-controlled CH660D electrochemical work station (CHI instruments Inc., USA) equipped with two compartment, three electrode cell. Platinum gauze used as current collector for the work electrode, platinum foil as the auxiliary electrode, and saturated calomel electrode as the reference electrode. The prepared active material powders was mixed with acetylene black, poly(tetrafluoroethylene) in the ratio as 85:10:5. A few drops of ethanol were added to form homogeneous slurry and the slurry was pressed and pasted on the platinum gauze with mass as 5 mg. all electrochemical measurements were carried out in a 6M KOH solution as the electrolyte.

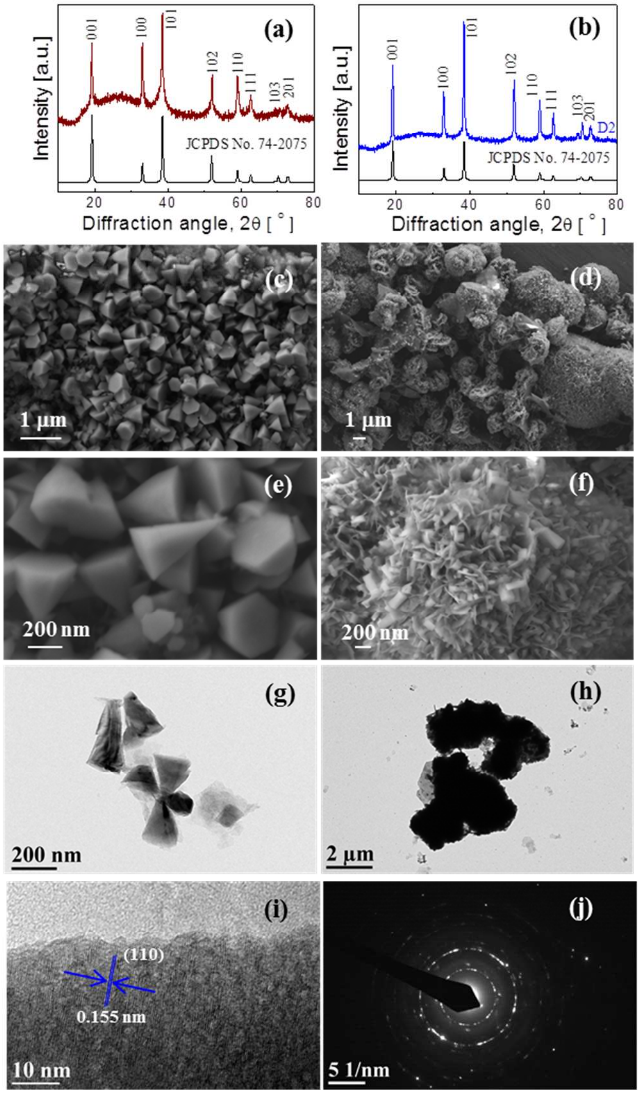

Fig.1. (a and b) XRD patterns, (c, d, e and f) SEM and (g, h and i) TEM images and (j) SAED pattern of the as-synthesized nickel hydroxide products: (a, c, e, g, and i) S1; (b, d, f, h, and j) S2.

Result and Discussion

The purity and crystallinity of as-synthesized products were examined by powder X-ray diffraction (XRD). The XRD-patterns of S1 and S2 are shown in **Fig. 1a** and **Fig. 1b**. Both diffraction patterns consist of prominent peaks at 19.5° (001), 32.55° (100), 38.95° (101), 51.5° (102) and 58.5° (110), readily indexed to pure hexagonal phase β-nickel hydroxide (P-3m1(164), JCPDS Card No. 74-2075; a=3.13, c=4.63), indicating the crystalline formation of pure $Ni(OH)_2$ materials. The morphologies of nickel hydroxide were investigated by FESEM and TEM. The FESEM image of S1 is shown in **Fig.1c**

and e. Geometrically cone-like particles scattered all over the spotting field. Each particle was determined to be about 100 nm in diameter and 200 nm in length. From SEM image of S2 shown in **Fig.1d and f**, numerous sheets were observed to be stacked together and constituted into large flower-like structures in the range of 400~800nm. The edges of nano-sheets can be clearly discerned along the macropores on the rough particle surfaces. TEM images of S1 and S2 are presented in the **Fig.1g** and **Fig.1h**, from which it can be seen that the particle size and the shape in TEM images agree with the SEM image result. The HRTEM image of nickel hydroxide nanoparticles (S1) is shown in **Fig.1i**, and the lattice spacing is discerned to be 0.155nm, corresponding to the (110) planes. Corresponding selected area electron diffraction pattern characterizations (SAED) of nickel hydroxide nanospheres were shown in **Fig.1j**. The disperse rings of were indexed to the crystal planes of (110), (111), (210), and (221), confirming the well-established crystalline feature.

XRD pattern were compared with JCPDS card No. 15-782 (show in **Fig.2a**), and the sample of S5 was revealed in composition of nickel carbonate. The peak at 14.95°, corresponding to (110) plane is more intense that others, implying the dominant orientation. The size of nickel carbonate particles was determined to be in the range of 40~80 nm from the observation in SEM and TEM images (shown in **Fig.2b** and **Fig.2c**). The clear dots in SAED-pattern (the inset of Fig. 2d) suggest that the nickel bicarbonate from hydrothermal reaction have a high order of crystallinity [18]. In HRTEM image shown in **Fig2d**, the fringe of S5 marked in white letters is measured to be 0.59 nm.

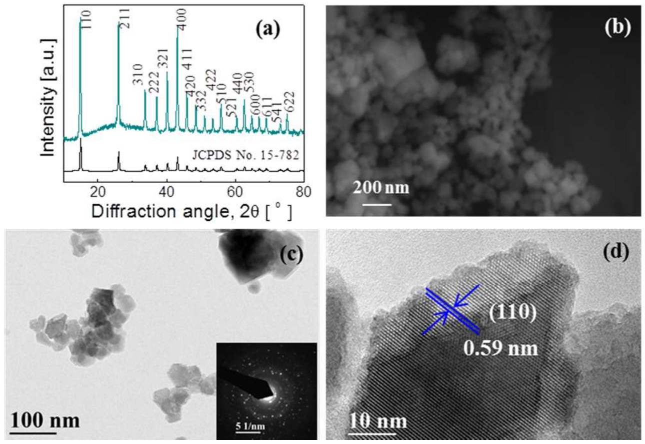

Fig.2 (a) XRD-pattern, (b) SEM, (c) TEM and (d) HRTEM image of the as-synthesized nickel bicarbonate (S5).

It was found that the urea play an important role in the fabrication of $Ni(OH)_2$ and $Ni(HCO_3)_2$. As shown in **Fig.3**, the XRD patterns of S3 and S4 indicate that both of them are composed of $Ni(OH)_2$ (JCPDS No. 74-2075) and $Ni(HCO_3)_2$ (JCPDS No. 15-782) when the amounts of urea is 6 mmol or 10 mmol. Based on the above results, the formation mechanism of nickel-based nanoparticles can be deducted as follows: urea decomposition resulted in releasing of CO_3^{2-} and NH_4^+, and their hydration process generated HCO_3^- and OH^-. At lower urea amount as 2 and 4 mmol, the generation of OH^- took the predominance and tend to precipitated $Ni(OH)_2$ particles (cone-like and flower-like forms). when urea amount were raised in the range of 6 mmol to 10 mmol, HCO_3^- and OH^- coexisted and precipitated mixtures of $Ni(OH)_2$ and $Ni(HCO_3)_2$. Pure $Ni(HCO_3)_2$ were synthesized while the amount of urea exceeds 20 mmol, at that time, HCO_3^- took the predominant amount in ureolysis. It is well-known that the formation of the anisotropic nanostructures with shape control in the crystallization process includes nucleation and growth. [19] In the present reaction system, lower amounts of urea might be advantageous the formation of $Ni(OH)_2$ nanoparticles. However, the involving of higher amounts of urea could enhance the nucleation rate of $Ni(OH)_2$ nanocrystals, resulting in the formation of sphereical nanoparticle aggregates. Compared with $Ni(OH)_2$, $Ni(HCO_3)_2$ has a unique crystal structure and different crystal growth habit, which might be beneficial for the formation of nanoparticles by such a hydrothermal route. Further investigation on the influence of urea's concentration and other experimental parameters on the formation of Ni-based nanostructures with different morphologies is still in progress. On the basis of observations, $Ni(OH)_2$ and $Ni(HCO_3)_2$ with different crystal structures and morphologies could be selectively synthesized through varying the initial urea amount by this method. The illustration of formation process is shown in **Scheme.1**.

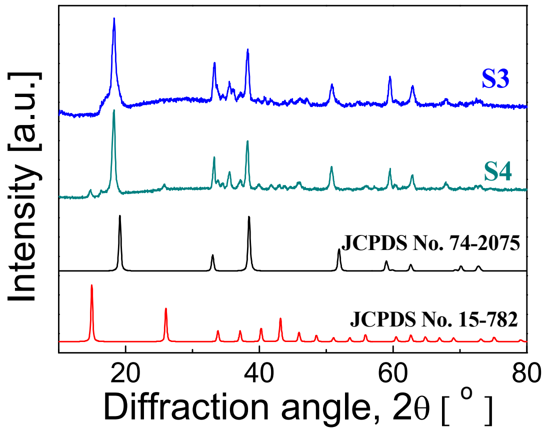

Fig.3. XRD patterns of s3 and s4 with PDF cards.

Surface area analysis of S1, S2 and S5 were investigated by nitrogen adsorption-desorption tests (the adsorption/desorption curves of S1, S2 and S5 are shown in **Fig.4a**). The surface area of flower-like large $Ni(OH)_2$ particles in S2 is about 45.7 $m^2\ g^{-1}$, which is much larger than the others. The minimum value was measured in the cone-like $Ni(OH)_2$ particles in S1 as 17.3 $m^2\ g^{-1}$. Besides the sphere-like $Ni(HCO_3)_2$ particles showed intermediate surface area value as 39.9 $m^2\ g^{-1}$. Majority parts of adsorption and adsorption overlapped, small hysteresis loops were observed above the value of P/P_0 in the range of 0.8~1, suggesting no mesopore formed in aggregation of nano particles.

The electrochemical performances were investigated in 6 M KOH with calomel reference electrodes. Cyclic voltammetry (CV) curves scanned at 10 mV s^{-1} are shown in **Fig. 4b**. All the CV curves comprise a pair of strong symmetry redox peaks, reflecting faradic pseudo-activity induced capacitance. The anodic peaks can be observed in the range of 0.25~0.4 V, which can be attributed to the oxidation of $Ni(OH)_2$ or $Ni(HCO_3)_2$ into NiOOH, while the catholic peaks at 0.0~0.1 V is related with the conversion of NiOOH back to $Ni(OH)_2$ or $Ni(HCO_3)_2$, the mechanism [20] is according to the following equation:

$$\mathrm{Ni(OH)_2 + OH^- \leftrightarrow NiOOH} + H_2O + e^-$$

$$\mathrm{Ni(HCO_3)_2 + 3OH^- \leftrightarrow NiOOH + 2HCO_3{}^- + H_2O + e^-}$$

The galvanic charge-discharge curves at the current density of 2 A g^{-1} within the voltage range of -0.2~0.5 V is shown in **Fig.4c**. Distinguished from the EDLC-type isosceles, the shape of charge/discharge curves are non-linear, the flat stage in the curves clearly demonstrates the pseudo-capacitance induced by faradaic charges. The specific capacitance can be calculated from CV curves and galvanic charge/discharge curves under the following equation:

$$\mathrm{C = S/2vm\Delta V,\ C} = \int I\Delta t/(m \cdot \Delta V)$$

Where S is the cumulus area of CV curves, v is the scan rate, m is the mass of active material (mg), I is the galvanic current (A g^{-1}), Δt is the charge/discharge time (sec), ΔV is the potential window (V). The corresponding specific capacitance measured by CV at 10mV s^{-1}, from S1, S2 and S5 is 683.7, 862.5, and 1429.3 F g^{-1}, respectively. Specific capacitance reflected from galvanic charge/discharge curves is in good agreement with the sequence, shown in **Fig.4c**. The massive surface area of flower-like structure enables its capacitive performance in S2 exceeds that of S1. The size-diminutive nickel bicarbonate spheres show the best performance in specific capacitance, this reason may be ascribe to the high electron-transfer efficiency induced by uniform dispersion of acetylene black in S5. Comparatively, current corrective acetylene black was difficult to go into the inner space of large flower-like particles partially compromised the electrochemical performance. Cyclic stability of S5 after 5000 repeated cycles is shown in **Fig. 4d**. During the stability measurements, there was no capacity shrink in the first 500 cycles. However, there is drastic capacity decrease from 500 to 200 cycles, and the capacity stabilized by 3750 cycles and only ~55% of the original specific capacitance was retained due to the detachment of nickel bicarbonate particles from the current collectors. CV plots for S5 at various scan rates are shown in **Fig. 4e**. From the CV curves, a linear increase in current density was observed with an increase in the scan rate range from 1 mV s^{-1} to 20 mV s^{-1}, indicating that the electrochemical process was surface confined [21]. In addition, within the increase of scan rate, the anodic peak potential and catholic peak potential shift positively and negatively, the capacitance decreases as elevated scan rates higher than 10 mv s^{-1}.

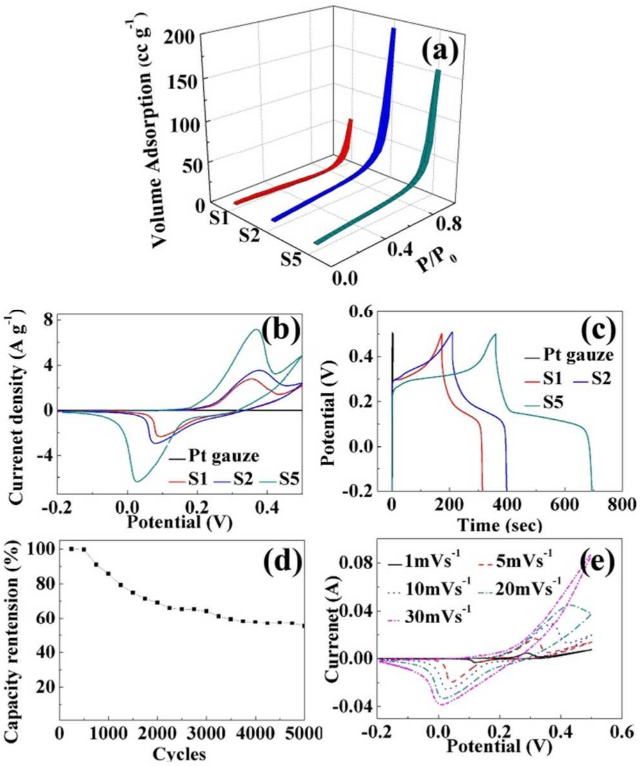

Fig.4 (a) the nitrogen adsorption/desorption curves of S1, S2 and S5; (b) the cyclic voltammetry curves; (c)galvanic charge/discharge curves of S1, S2, and S5; (d) the capacitance stability of S5, (e) cyclic voltammetry of S5 at different scan rates.

We also have tried the assembling of supercapacitors according to the papers reported. [22-24] The active materials (active carbon as anode and nickel bicarbonate as cathode) were casted on the nickel foam with the density as 5 mg cm^{-2} (1 cm x 1 cm). The asymmetric supercapacitor was assembled by pressing the 2 electrodes into cell, which was separated by a nylon paper. The electrolyte was 6 M KOH aqueous solution. Fig. 5 shows the cyclic voltammertrical and galvanic charge/discharge curves of asymmetric cell. The rudimentary measured capacitance of as-made assymmetric cell is about 64.2 F g^{-1} in the scan range of 0~1.5 V at the scan rate of 1 mV s^{-1}, which is higher than the reported value as 37 F g^{-1} in NiO/active carbon asymmetric cell. [25] The above results suggest that the as-synthesized $Ni(HCO_3)_2$ nanoparticles is promising electrode material.

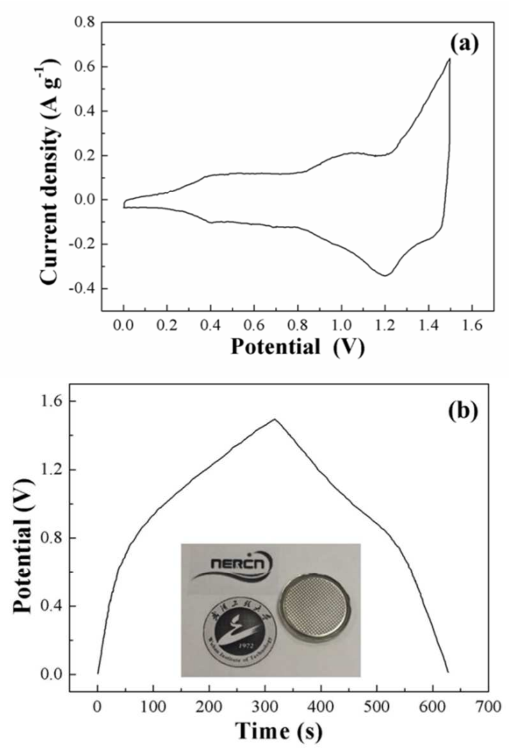

Fig.5 (a) cyclic voltammertrical curve of asymmetric cell at 1 mV s^{-1}, (b) galvanic charge/discharge curves of assembled asymmetric cell at 1 A g^{-1}.

Conclusions

In this communication, cone-like, flower-like nickel hydroxide and sphere-like nickel bicarbonate was facilely synthesized without surfactants. The crystal phase, structure, surface area, and correlated electrochemical properties of the as-synthesized products were systematically investigated. The surface areas of obtained materials are measured to be 17.3 m^2 g^{-1}, 45.7 m^2 g^{-1} and 39.9 m^2 g^{-1}, respectively and the correlated electrochemical performance was systematically compared. The maximum specific capacitance was measured to be 1429.3 F g^{-1} in sphere-like nickel bicarbonate, suggesting their potential application as supercapacitor electrode materials.

Notes and references

[a] *National Engineering Research Center for Nanotechnology, Shanghai,,200241, P.R. China.*
[b] *School of Chemistry and Environmental Engineering, Wuhan Institute of Technology, Xiongchu Avenue, Wuhan, 430073, P. R. China.*
**Correspondence to: G. Cheng (gchenglab@163.com), D. He (hdn_nercn@163.com), and R. Chen (rchenhku@hotmail.com)*

1 B.E.Conway, Electrochemical supercapacitors: scientific fundamentals and technological applications, Plenum Publishers, New York, 1st edn., 1999.
2 X. Wang, X. Lu, B. Liu, D. Chen, Y. Tong and G. Shen, Adv. Mater., 2014, DOI: 10.1002/adma.201400910.
3 Y. Yan, T. Kuila, N. H. Kim and J. H. Lee, Carbon, 2014, 74, 195.
4 L. Mai, F. Yang, Y. Zhao, X. Xu, L. Xu and Y. Z. Luo, Nat Commun, 2011, 2, 381.
5 K. M. Hercule, Q. Wei, A. M. Khan, Y. Zhao, X. Tian and L. Mai, Nano Lett., 2013, 13, 5685-5691.
6 D. S. Kong, J. M. Wang, H. B. Shao, J. Q. Zhang and C. N. Cao, J. Alloy. Compd., 2011, 509, 5611.
7 W.-K. Hu, X.-P. Gao, D. Noréus, T. Burchardt and N. K. Nakstad, J. Power Sources, 2006, 160, 704.
8 H. Li, S. Liu, C. Huang, Z. Zhou, Y. Li and D. Fang, Electrochim. Acta, 2011, 58, 89.
9 Y. Kido, K. Nakanishi, N. Okumura and K. Kanamori, Microporous Mesoporous Mater., 2013, 176, 64.
10 M. S. Wu and K. C. Huang, Int. J. Hydrogen Energy, 2011, 36, 13407
11 Y. Miao, L. Ouyang, S. Zhou, L. Xu, Z. Yang, M. Xiao and R. Ouyang, Biosens. Bioelectron., 2014, 53, 428.
12 R. Acharya, T. Subbaiah, S. Anand and R. P. Das, J. Power Sources, 2002, 109, 494.
13 T. Subbaiah, R. Mohapatra, S. Mallick, K. G. Misra, P. Singh and R. P. Das, Hydrometallurgy, 2003, 68, 151.
14 X. C. Song, X. Wang, Z. A. Yang and Y. F. Zheng, Mater. Lett., 2011, 65, 2348.
15 Q. Li, H. Ni, Y. Cai, X. Cai, Y. Liu, G. Chen, L.-Z. Fan and Y. Wang, Mater. Res. Bull., 2013, 48, 3518.
16 C. Coudun, F. Grillon and J.-F. Hochepied, Colloid Surfaces A, 2006, 280, 23.
17 X. Liu and L. Yu, J. Power Sources, 2004, 128, 326.
18 H. J. Liu, T. Y. Peng, D. Zhao, K. Dai and Z. H. Peng, Mater. Chem. Phys., 2004, 87, 81.
19 Y. C. Cao, J. Am. Chem. Soc., 2004, 126, 7456.
20 J. Sun, Z. Li, J. Wang, Z. Wang, L. Niu, P. Gong, X. Liu, H. Wang and S. Yang, J. Alloys Compd., 2013, 581, 217.
21 T. Kuila, P. Khanra, N. H. Kim, J. K. Lim and J. H. Lee, J. Mater. Chem. A, 2013, 1, 9294.
22 J. Huang, P. Xu, D. Cao, X. Zhou, S. Yang, Y. Li and G. Wang, J. Power Sources, 2014, 246, 371.
23 J. Yan, Z. Fan, W. Sun, G. Ning, T. Wei, Q. Zhang, R. Zhang, L. Zhi and F. Wei, Adv. Funct. Mater., 2012, 22, 2632.
24 Y. Tang, Y. Liu, S. Yu, Y. Zhao, S. Mu and F. Gao, Electrochim. Acta, 2014, 123, 158-166.
25 D. Wang, F. Li and H. Cheng, J. Power Sources, 2008, 185, 1563-1568.